Molten Salt Shielded Synthesis of Monodisperse Layered CaZnOS-Based Semiconductors for Piezophotonic and X-Ray Detection Applications

Yuantian Zheng, Xu Li, Ronghua Ma, Zefeng Huang, Chunfeng Wang, Mingju Zhu, Yangyang Du, Xian Chen, Caofeng Pan, Bohan Wang, Yu Wang, and Dengfeng Peng*

CaZnOS-based semiconductors are the only series of material system discovered that can simultaneously realize a large number of dopant elements to directly fulfill the highly efficient full-spectrum functionality from ultraviolet to near-infrared under the same force/pressure. Nevertheless, owing to the high agglomeration of the high temperature solid phase manufacturing process, which is unable to control the crystal morphology, the application progress is limited. Here, the authors report first that CaZnOS-based fine monodisperse semiconductor crystals with various doping ions are successfully synthesized by a molten salt shielded method in an air environment. This method does not require inert gas ventilation, and therefore can greatly reduce the synthesis cost and more importantly improve the fine control of the crystal morphology, along with the crystals' dispersibility and stability. These doped semiconductors can not only realize different colors of mechanical-to-optical energy conversion, but also can achieve multicolor luminescence under low-dose X-ray irradiation, moreover their intensities are comparable to the commercial NaI:Tl. They can pave the way to the new fields of advanced optoelectronic applications, such as piezophotonic systems, mechanical energy conversion and harvesting devices, intelligent sensors, and artificial skin as well as X-ray applications.

1. Introduction

Mechanoluminescence (ML) is a photon emission phenomenon in which luminescent objects directly convert mechanical energy into light emissions. As smart materials, ML semiconductors have attracted extensive attention and have made significant progress in recent years, owing to their important potential applications in the fields of piezophotonics,

light-generators, stress sensing, flexible, and stretchable displays, mechanical energy harvesting and conversion, and integrated tribotronic devices.[1–10] They can emit light and are regarded as smart creatures (like *Noctiluca scintillans* shining by the impact of waves) when exposed to external momentary stimuli.[11–14]

Many materials discovered in nature provide the capability to emit light in response to dynamic forces/pressures, whether natural or man-made, such as quartz and sugar.[15,16] There are two categories of ML materials systems: organics and inorganics;[17,18] however, most of the current organic ML materials emit photons by releasing energy from the breaking of chemical bonds, resulting in a poor recovery, or requiring recrystallization to reproduce the light emitting process. Inorganic ML materials can be divided into insulators and semiconductors. As one of the II–VI ML semiconductors, ZnS has very interesting mechanical-to-optical properties, owing to its labile changing elastic and plastic deformation crystal structure, as well as its special piezoelectric and friction characteristics.[19–24] The novel ML properties of ZnS-based composites have aroused broad research interest in recent years.[1,26–31] Semiconductors such as doped ZnS, can directly convert mechanical energy into light energy, providing broad application prospects in the fields of stress/strain sensing, wind/droplet driving displays,

Y. Zheng, X. Li, R. Ma, Z. Huang, C. Wang, M. Zhu, D. Peng
Key Laboratory of Optoelectronic Devices and Systems of Ministry of Education and Guangdong Province
College of Physics and Optoelectronic Engineering
Shenzhen University
Shenzhen 518060, China
E-mail: pengdengfeng@szu.edu.cn
Y. Du, X. Chen
College of Materials Science and Engineering
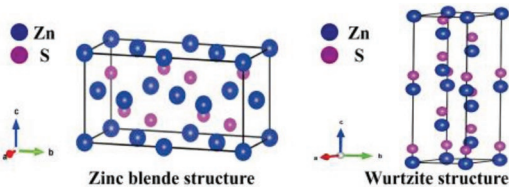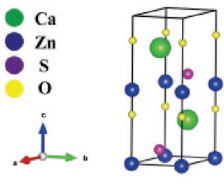Shenzhen University
Shenzhen 518060, China

The ORCID identification number(s) for the author(s) of this article can be found under https://doi.org/10.1002/smll.202107437.

C. Pan
CAS Center for Excellence in Nanoscience
Beijing Key Laboratory of Micro-nano Energy and Sensor
Beijing Institute of Nanoenergy and Nanosystems
Chinese Academy of Sciences
Beijing 100083, China
B. Wang, Y. Wang
International Collaborative Laboratory of 2D Materials for Optoelectronics Science and Technology of Ministry of Education
Institute of Microscale Optoelectronics
Shenzhen University
Shenzhen 518060, China

Table 1. Physical properties comparisons of ZnS and CaZnOS.[36] ZnS can only be effectively doped with copper and manganese to form ML, whereas CaZnOS can be not only doped with copper and manganese to form luminescence, but also with various lanthanide ions.

	ZnS	CaZnOS
Direct semiconductor	Yes	Yes
Piezoelectric constants	8 pmV^{-1}	38 pmV^{-1}
Band gap	3.7 eV	3.67 eV
Crystal structure	Zinc blende structure / Wurtzite structure	
Luminescent dopants	Cu, Mn	Transition metals: Cu, Mn, etc Lanthanide ions: Eu, Pr, Tb, Sm, etc
Dopant concentration	<5%	Transition metals: <5% Lanthanide ions: <10%
Atmosphere	Vacuum, N_2-O_2, H_2	Ar, N_2, H_2-Ar, H_2-N_2

and commodity anti-counterfeiting. However, it can only realize copper and manganese pioezophotonic emissions. As derivatives of zinc sulfide, CaZnOS[32–34] semiconductors are of great interest as inorganic ML materials, and have been intensively studied. CaZnOS has a band gap similar to that of zinc sulfide, but has a piezoelectric coefficient four times higher than that of zinc sulfide. CaZnOS has two cation sites, Ca and Zn; the ionic radius of Ca is similar to that of Ln^{3+} ions, whereas Zn is similar to transition ions such as Mn and Cu. Accordingly, as the most efficient inorganic ML semiconductor, the host can realize good crystal compatibility and high-efficiency ML, as well as full spectral emissions from visible to near IR light[35] under the same force, making it advantageous for practical applications in sensing and mechanical-to-optical energy conversions. Their physical properties are presented in **Table 1**.

In general, as a light-emitting or sensing unit, one particle acts as an independent receptor; a mechanical response light-emitting sensor is active, and does not require external power or electrodes. Therefore, the sensing and light-emitting performance greatly depends on the shape and orientation of the particle itself, especially for anisotropic ML crystals. At present, the preparation of CaZnOS is an inert gas protection solid-state method (SSM).[36,37] The high-temperature SSM can easily lead to the direct agglomeration of crystals and irregular morphologies. Some alkaline earth oxide ions form flux, but can lead to

serious chemical and physical agglomeration of particles. After firing, the obtained block requires mechanical ball milling; this can easily destroy the original growing crystal shape, and the particle size distribution is very wide and uneven. Therefore, despite the significant progress that has been made, there is an urgent need to develop a controllable, large-scale, and low-cost method for obtaining high-quality ML crystals.

The molten salt shielded (MSS) method is a method for growing crystals at relatively low temperatures (lower than those of the traditional SSMs) by using salt with a low melting point. It does not need to react in an inert gas atmosphere. At present, many popular materials have been synthesized by this method; for example, large-scale Ti$_3$ZnC$_2$, InP, and CdS quantum dots have been synthesized using molten methods, thereby providing a green and feasible route for the preparation of oxidation-prone materials.[38–42] Depending on the intrinsic melting point of the salt, the alternative temperature ranges from 100 to 1000 °C, allowing access to a broad range of inorganic crystalline materials.

In this work, as a novel approach, we synthesized CaZnOS-based ML semiconductor materials using an MSS method, the process is described in **Figure 1**. This method only needs to be synthesized in air without ventilation, largely reducing the cost; in addition, the flake single crystal synthesized by our method has a regular shape, uniform size distribution, and high
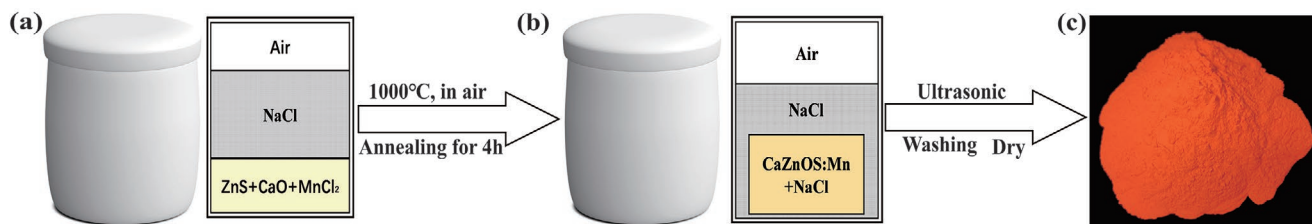

Figure 1. Schematic diagram of in air molten salt process for CaZnOS: a) Filling of samples in corundum crucible before reaction; b) placing corundum crucible in the furnace and annealing at 1000 °C in air for 4 h, washing NaCl in reaction product with deionized water, drying the washed reaction product, and finally obtaining CaZnOS:Mn crystals; c) a photograph under an UV lamp.
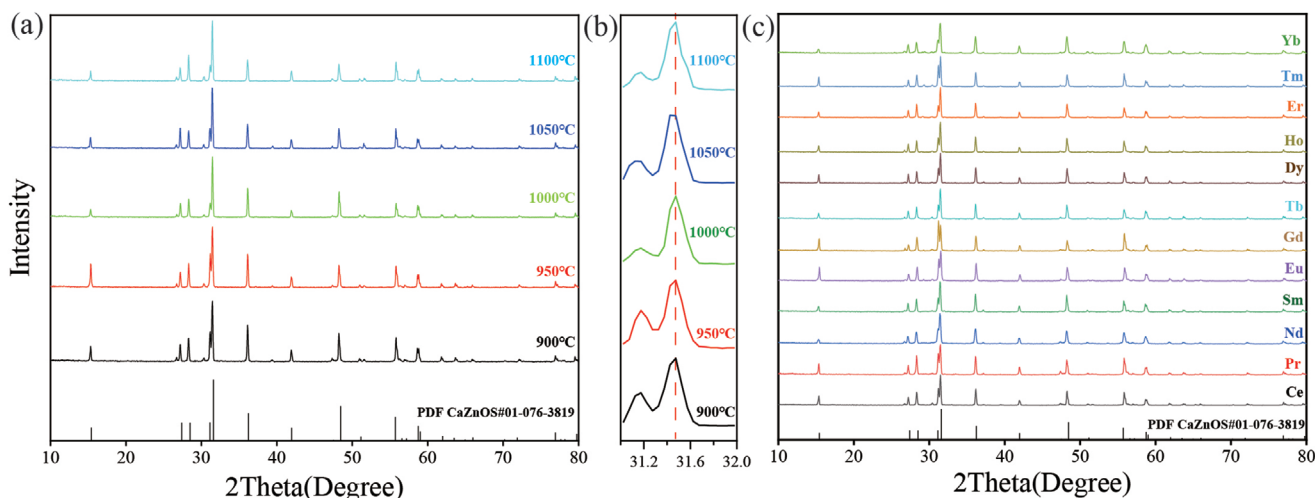
Figure 2. X-ray diffraction (XRD) spectra of the samples prepared by molten salt shielded (MSS) method: a) the XRD of CaZnOS samples doped with Mn ions annealed at 900, 950, 1000, 1050, and 1100 °C; b) refined XRD peaks of CaZnOS:Mn located from 31° to 32°; c) XRD of CaZnOS samples doped with lanthanide ions annealed at 1000 °C.

crystallization. It is very convenient for fabricating coatings on the surfaces of printed matter, handicrafts, or various structures for research on strain sensing, anti-counterfeiting, information security, and piezoelectric photonics devices, thereby paving the way for large-scale industrial applications. At the same time, the transition metal and lanthanide ion-doped semiconductor single crystal synthesized by this MSS has many luminescent properties, and can actively regulate its photoluminescence (PL) and X-ray excited luminescence (XEL). Therefore, as an important functional optical material, it can expand the research scope of traditional semiconductors, such as advanced flexible optoelectronic applications, and allow for the development of new light generators, as well as piezo-photonic materials and devices of third-generation semiconductors.[18,43,44]

2. Results and Discussion

Powder X-ray diffraction (XRD) characterizations were performed to evaluate the crystal structure of the obtained crystals. **Figure 2**a shows the XRD pattern comparisons between the CaZnOS:Mn powders fired at different temperatures and a standard powder diffraction file (PDF) from card No. #01-076-3819. All the standard diffraction peaks are well aligned with that of our samples, indicating that the CaZnOS phase is successfully formed. In all of the powders fired from an evaluated temperature of 900–1100 °C, no dopant impurity (except trace ZnS phases) diffraction peaks are detected, indicating that the dopant of Mn^{2+} does not change the structure of the CaZnOS host; all of the dopants are evenly integrated into the crystal, and doped successfully. Considering the coordination number and ionic radius, Mn^{2+} (Coordination Number (CN_4), 0.66 Å) can easily replace the position of Zn^{2+} (CN4, 0.60 Å).[45] Figure 2b shows the peak shift of the strongest diffraction from 31° to 32° in the 2θ range. As the temperature increases, the peak position does not evidently move. Figure 2c shows the XRD comparisons between different Ln^{3+} lanthanide-doped CaZnOS crystals synthesized at 1000 °C and a standard PDF card of CaZnOS,

showing that the CaZnOS phosphors doped with different lanthanide ions synthesized by the molten salt method are also single-phase, that no new lanthanide-ion oxide impurity phases are produced in the matrix, and that Ln^{3+} mainly replaces the position of Ca^{2+} sites owing to the similar ion radii of the lanthanide ions and Ca^{2+} (CN6, 1.00 Å). CaZnOS is a non-centrosymmetric structure with a space group $P6_3mc$, and is composed of homogeneously folded hexagonal ZnS and CaO layers. The arrangement of these layers comprises $[ZnOS_3]$ tetrahedrons arranged in parallel, thereby generating polarization and piezoelectric behaviors.[46,47] In addition to the ability to synthesize the above-mentioned monophasic luminescent materials, this MSS method can also be used to synthesize more complex structures, such as oxysulfides and sulfide heterojunctions. Mn-doped ZnS/CaZnOS heterojunctions are successfully obtained by this method, and XRD diffraction measurements prove that the desired phases are also synthesized (Figure S1, Supporting Information). Notably, all lanthanide-doped CaZnOS phosphors synthesized in air by the MSS method are achieved for the first time; this approach is convenient for obtaining uniform crystals and can greatly reduce the synthesis cost, making it beneficial for large-scale industrial operation.

Mechanoluminescent crystals are often used as stress sensors and the single particles are separate sensors; thus, the morphologies and sizes of the crystals will have great influences on the performance of their sensing properties. **Figure 3** shows the scanning electron microscopy (SEM) images of the CaZnOS crystals doped with manganese ions synthesized at different temperatures using the MSS method. The SEM images represent samples annealed at different temperatures from 900 to 1100 °C.

Generally, compared with the traditional solid-phase method, the phosphor synthesized by the MSS method has a regular and controllable morphology, and the crystals generally exhibit a sheet-like structure. Moreover, the SEM images show that the samples tend to grow into a flat shape at a lower temperature. As the temperature increases, the crystals gradually form a full round drum-like crystal with evident layered stacking structure.
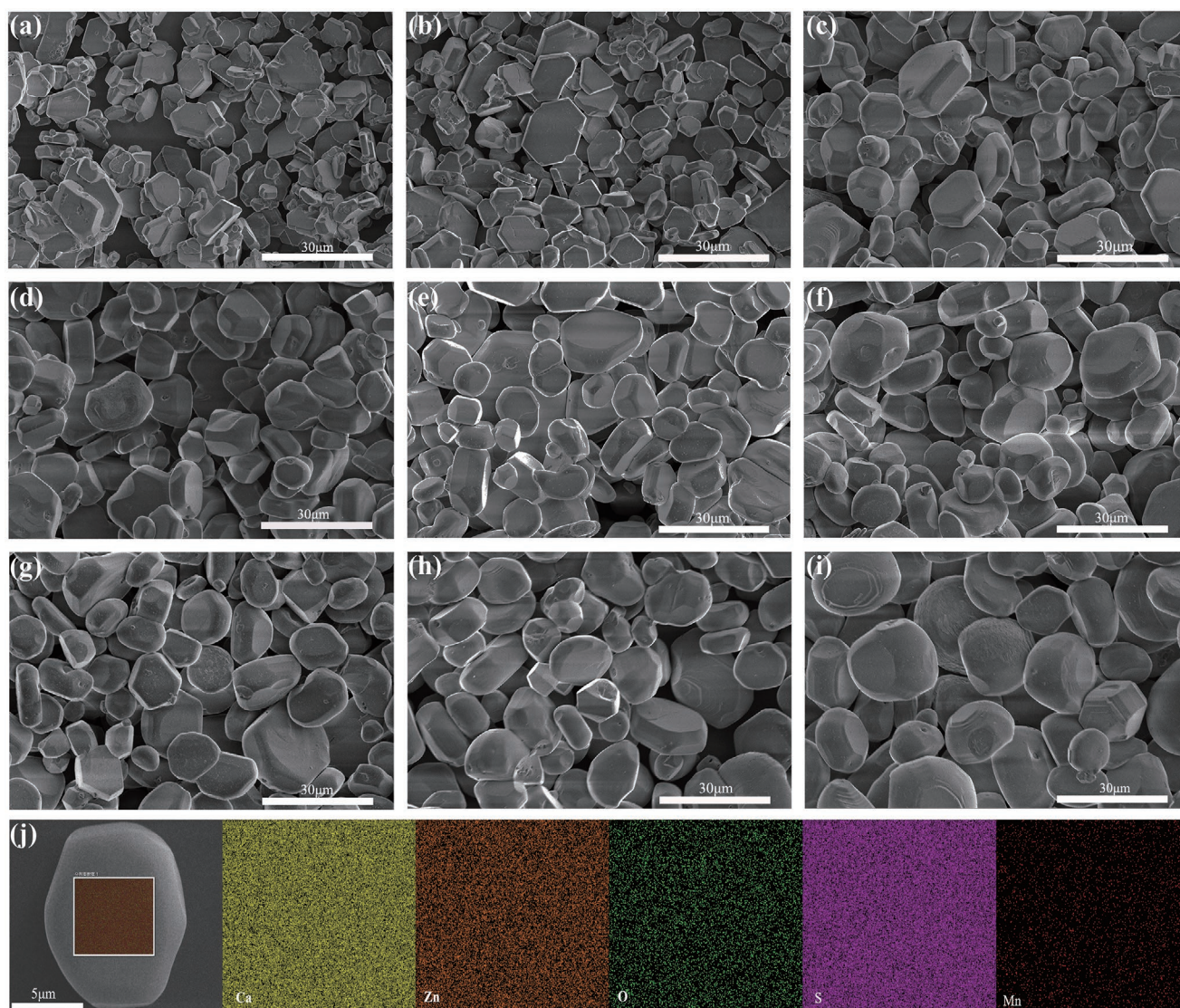
**ADVANCED
SCIENCE NEWS**
www.advancedsciencenews.com

**NANO · MICRO
small**
www.small-journal.com

Figure 3. Scanning electron microscopy (SEM) images of the samples prepared by MSS method a–i): the CaZnOS samples doped with Mn ions annealed at 900, 950, 1000, 1010, 1020, 1030, 1040, 1050, and 1100 °C, respectively. Different from the traditional solid-state method, our crystal has high crystallinity and dispersion, the crystal surface is smoother than the samples prepared by traditional solid-state reaction. j) EDS images of Mn doped CaZnOS.

In addition to the Mn^{2+} ions doped crystals, the lanthanide ion-doped samples also have similar morphological characteristics (Figure S2, Supporting Information), for example, the SEM and energy dispersive X-ray spectroscopy (EDS) spectra of the CaZnOS doped with lanthanide ions such as Gd^{3+} and Ho^{3+} ions. It can be seen that our obtained samples are still regular and generally exhibit a layered-like structure. The EDS element map image shows that Ca, Zn, O, S, and Gd/Ho atoms are uniformly distributed throughout the selected area. We applied the focused ion beam technique to get a proper thin sample and further carried out characterization through a high-resolution scanning transmission electron microscopy (STEM) (Figure S3, Supporting Information). We finally confirm our sample is single crystalline structure. During the course of the experiment, we found that the samples doped with Ln^{3+} ions were harder than the samples doped with Mn^{2+} before washing

with deionized water, and agglomerated more compactly in the crystalline molten salt. Therefore, some samples would slightly grind the whole sample into small pieces before washing.

Semiconductor doping through a small amount of luminescent center transfers the energy absorbed by the host to the doped ions through energy transfer. For example, zinc sulfide doped with manganese elements can achieve good PL performance through a small amount of doping. To study the luminescence properties of CaZnOS samples obtained under different synthesis conditions and different doping ions, we conducted PL tests. We systematically studied the PL spectra, including the excitation and emissions of the CaZnOS:Mn crystals synthesized at different temperatures, as shown in **Figure 4**. It can be seen that as the temperature increases, the integrated PL intensity continues to increase. This is because the increase in temperature is conducive to
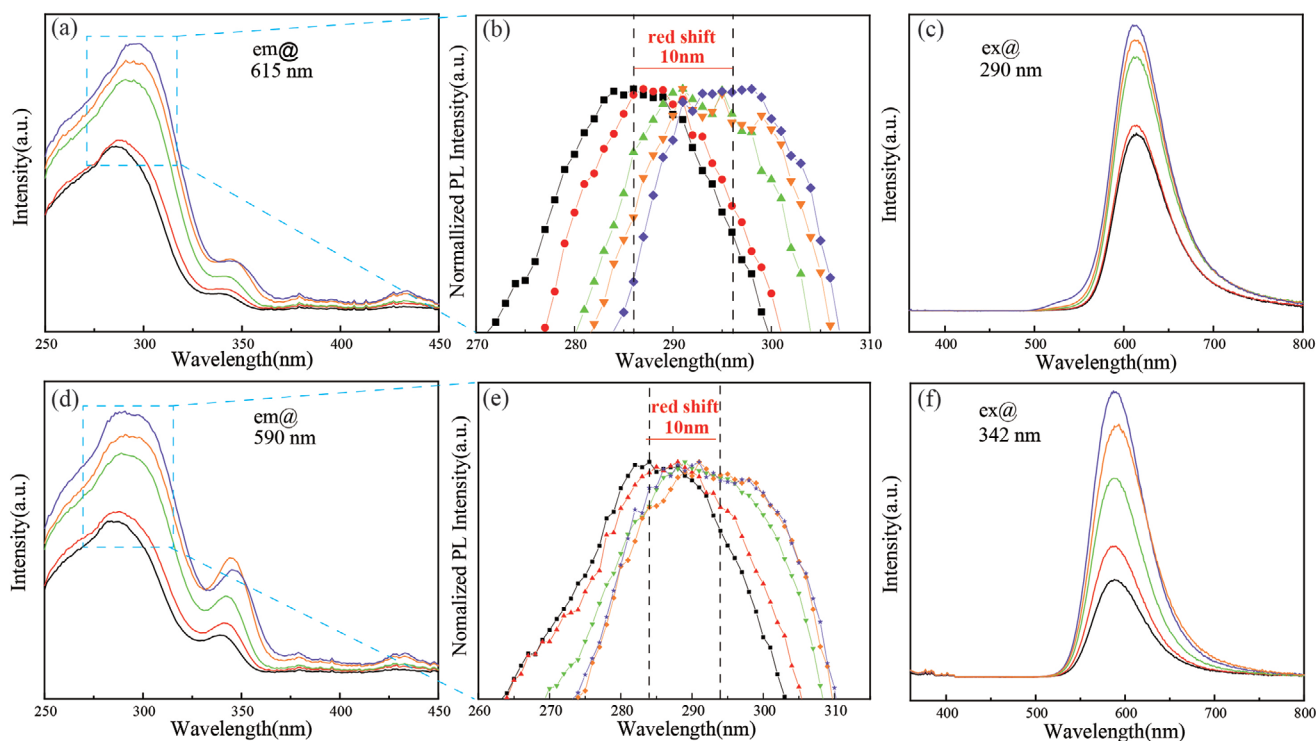
**ADVANCED
SCIENCE NEWS**
www.advancedsciencenews.com

NANO · MICRO
small
www.small-journal.com

Figure 4. Photoluminescence spectra of CaZnOS:2% Mn crystals prepared under the different temperatures (from bottom to top is 900, 950, 1000, 1050, and 1100 °C): a,d) the excitation emission spectra monitored by 615 and 590 nm, respectively, b,e) the corresponding magnified normalized photoluminescence spectra, showing the red shift, and c,f) the excitation spectra of 290 and 342 nm, respectively. We notice that the excitation peak is quite different from the traditional solid-state method. At the same time, for the excitation peak, the synthesis temperature can cause the shift of manganese luminescence peak, which has not been observed in the previous research methods. Our method can adjust the spectral characteristics more flexibly.

the diffusion of Mn^{2+} (CN4, 0.66 Å) more effectively into the lattice, theoretically replacing the positions of the Zn^{2+} (CN4, 0.60 Å) ions. As the doping concentration of Mn^{2+} is fixed at 2 mol% (relative to ZnS), we observe a strong band emission at 615 nm, as derived from the strong $^4T_1(^4G) \rightarrow {}^6A_1(^6S)$ emission of Mn^{2+}; this is consistent with previous reports.[45] The corresponding excitation spectrum, monitored at 615 nm, is shown in Figure 4a. At high temperature, a small amount of manganese is actually not excluded from entering the calcium site, resulting in the shift of the excitation peak (Figure 4a). The red shift of the excitation peak may also be related to the anisotropy of the crystal. We found that the stacking of layered crystal particles becomes thicker with the increase of temperature, resulting in a change in the coordination transmission of manganese ions. Interestingly, with the change in temperature, the wavelength of the emission spectra is red-shifted. We normalize at the 270–310 nm range of the spectrum to make it easier to see this shift as a red-shift of ≈10 nm, as shown in Figure 4b. Notably, we need to spread a layer of NaCl on top of the reactants before placing the mixtures into the muffle furnace and heating. The melting point of the NaCl is ≈801 °C. After melting at a high temperature, it can not only isolate oxygen and prevent Mn^{2+} and S^{2-} ions from being oxidized, but can also provide a liquid reaction environment. Increasing the reaction rate is conducive to a more complete reaction. However, the molten salt volatilizes to an extent at high temperatures; this phenomenon has been noticed by us, especially after

the temperature reaches 1100 °C. Accordingly, a large amount of NaCl should cover the upper layer of the mixtures to prevent the Mn^{2+} ions from becoming oxides such as MnO_2. Once this reaction takes place when the temperature exceeds the molten salt NaCl boiling point, the former manganese oxide (high valence manganese) quenches the luminescence of the sample, and may reduce the intensity of the luminescence as a whole. The volatilization of molten salt increases the Mn^{2+} concentration in the reaction environment, shifting the excitation peak of the main lattice from 284 (900 °C) to 294 nm (1100 °C) to a longer wavelength. More interestingly, a new excitation peak at 342 nm of the long-wavelength UV spectrum is observed in the sample synthesized by the MSS method of CaZnOS:Mn. This provides more convenient approaches to the multi-wavelength excitation of samples. The addition of chloride ions may be involved in the energy transfer in the luminescence process, and the defect luminescence caused by them is overlapped with the spectra of manganese. Therefore, when we monitor different wavelengths, the excitation spectra are different. This phenomenon may also be caused by various factors or different occupations of manganese. It cannot be ruled out that a small amount of manganese may enter the calcium cation site, making the coordination field around the manganese ions different. The other excitation peaks at ≈398 and 496 nm can be attributed to the electronic transitions of $^6A_1(^6S) \rightarrow {}^4T_2(^4D)$ and $^6A_1(^6S) \rightarrow {}^4T_2(^4G)$. As shown in Figure 4a, the intensity of the excitation band of the main lattice is much stronger than that

ADVANCED
SCIENCE NEWS
www.advancedsciencenews.com
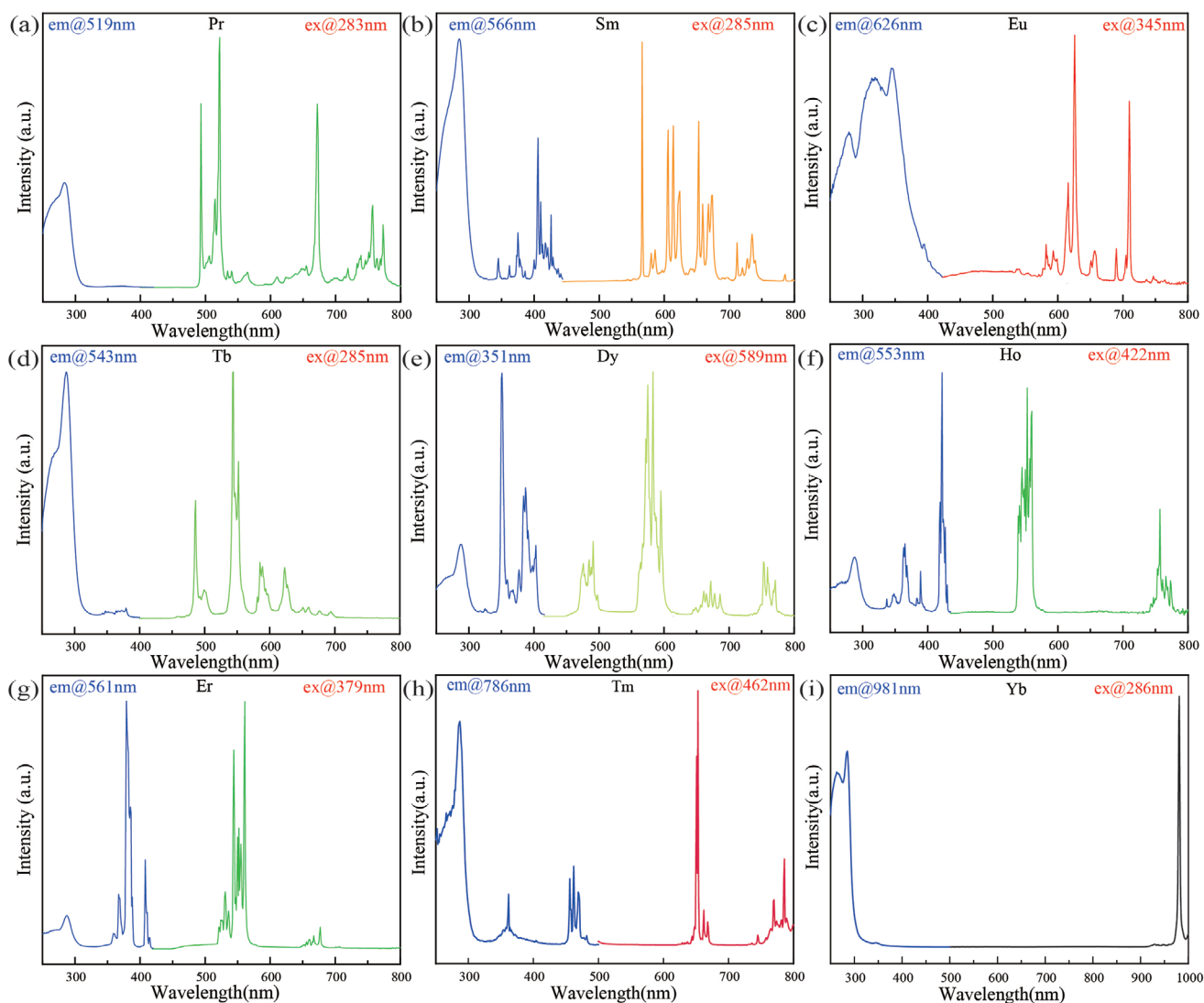
NANO · MICRO
small
www.small-journal.com

Figure 5. Room temperature excitation (blue line) and emissions (corresponding to the light-emitting color line) spectra of CaZnOS microcrystals doped with different lanthanide elements a) Pr, b) Sm, c) Eu, d) Tb, e) Dy, f) Ho, g) Er, f) Tm, and i) Yb), showing our method can not only realize host sensitization, but also realize self-sensitized luminescence of lanthanides, which is different from the previous traditional methods.

of the latter, indicating that the energy is effectively transferred from the main lattice of the crystalline host to the Mn^{2+} ions. We found that the crystals grown by molten salt method have higher quantum yield (QY) than those grown by traditional SSM. As we can see, the CaZnOS:Mn (Figure 1c) can emit strong red fluorescence under UV lamp irradiation. We tested the QY of the phosphor under 290 nm excitation, the spectra are shown in Figure S4, Supporting Information. The QY of the phosphor synthesized by MSS method is 57.45%, this value is much higher than that of the sample prepared by solid state reaction method (CaZnOS:Mn, QY = 27.3%),[35] the high QY is attributed to the higher crystallinity and larger and uniform grain size of our samples.

In addition, we also investigated the PL spectra of the lanthanide ions in the CaZnOS semiconductor, as shown in **Figure 5**, where the blue line represents the excitation spectra, and the other lines are the corresponding emission spectra.

To scan the luminescence peak in the visible region and its extension, we recorded the PL spectra for all the lanthanide ion-doped samples from 250 to 800 nm with a test slit of 1 nm, step size of 1 nm, and dwell time of 0.2 s. We selected a part of the excitation spectra from 250 to 500 nm for comparing the similarities and differences between the matrix excitation and intrinsic excitation of the different lanthanide ions, as shown in Figure 5. The complete excitation spectra are shown in Figure S5, Supporting Information. Because the ion radius of Ln^{3+} is similar to that of Ca^{2+} ions, lanthanide ions tend to replace calcium sites independently in CaZnOS crystals. The excitation spectra of the different lanthanide ions are distributed in different positions, some near 280–290 nm, and some in the longer wavelength region, such as blue light; for example, the dominant excitation spectra of a crystal doped with Eu^{3+}, Tb^{3+}, and Yb^{3+} are located at ≈290 nm. This originates from the CaZnOS host, indicating that the energy

transfer efficiency from the host to the dopant is relatively high, whereas other samples such as the Pr^{3+}, Dy^{3+}, Ho^{3+}, and Er^{3+} doping samples mainly show a longer excitation characteristic, as respectively determined by the characteristic f–f transition peak of the lanthanide dopant. Neutrally, the samples of Sm^{3+} and Tm^{3+} balance to an equal level; that is, they can be effectively excited by both the matrix and lanthanide ions themselves, as related to the doping and defect energy levels formed in the matrix.[48,49] The energy level matching and excitation energy transfer efficiency are related to the configuration of the final excitation spectrum. These provide rich options for flexible excitation and the manufacturing of semiconductor-integrated displays in the future. The different spectral peak positions correspond to transitions of different energy levels. We organized them into tables; details can be found in the appendix (Table S2, Supporting Information).

As lanthanide ion elements also emit light in IR light, providing options for real applications including therapy, laser, bioimaging, monitoring, and IR communication, we also investigated the PL emissions of Nd-, Pr-, Yb-, and Er-doped CaZnOS, respectively, as shown in Figure S6, Supporting Information. Nd doping has received great attention as an efficient near-IR luminescent dopant.[37,50] Therefore, we successfully synthesized doped micro single crystals and synthesized CaZnOS doped with Nd, consistent with previous literature reports, as shown in Figure S7, Supporting Information. The transition metals of Cu-and Pb-doped crystals were also successfully obtained by using the MSS method; the doped samples show green and deep blue emissions, respectively, and their characteristic luminescence is obtained even with a low concentration of dopants, for example, 0.1% Cu and 0.1% Pb mol doping, respectively. In addition, doping characteristic emissions (rather than those of the matrix) can be seen (Figures S8,S9, Supporting Information). By using this method, we can realize the intrinsic luminescence of all luminescent ions, as long

as the dopants can be successfully doped into the crystal. To further demonstrate that our method can enrich the PL emissions of various structures, such as heterojunction structures, the PL spectra of the ZnS-CaZnOS:Mn heterojunction synthesized by the MSS method as shown in Figure S10, Supporting Information and its corresponding strong emissions can be observed under UV light excitation (especially at 290 nm). The crystals synthesized by the high-temperature SSM have the characteristics of uniformly dispersed crystal particles. After treatment in the high-temperature solid-state molten salt, the crystal has a smooth crystal surface, and the crystal surface with the lowest energy is mainly exposed outside the crystal, thereby resisting the corrosion of ions in the environment; therefore, it has the chemical characteristics of a high temperature, and can be stored in air or water for a long time without decomposition. The samples fired using the MSS method are chemically stable in the ambient environment. As shown in Figure S11, Supporting Information, we retested the PL spectra of the CaZnOS:Mn samples after 6 months; the PL configuration and intensity of the samples prepared by the MSS method are basically the same as when first synthesized.

After considering the PL, we studied the ML. **Figure 6** shows the ML spectra of different doped (Mn^{2+} and Ln^{3+}) CaZnOS synthesized by the MSS method. Figure 6a shows the ML spectra of CaZnOS:Mn synthesized at 1000 °C under different forces. Figure 6b is the integral intensity diagram from Figure 6a. It can be seen that as the force increases, the luminous intensity also increases; this is different from the behavior of previously reported samples annealed by the traditional SSM, and may be caused by the anisotropy of the uniform sheet-like crystals. The samples emit light more easily under higher pressure, so the overall luminescence enhancement trend is more evident. We further conduct ML test under high pressure (200–1000 N), the ML intensity integral of phosphor exponentially increase with the applied force. (Figure S12, Supporting Information).
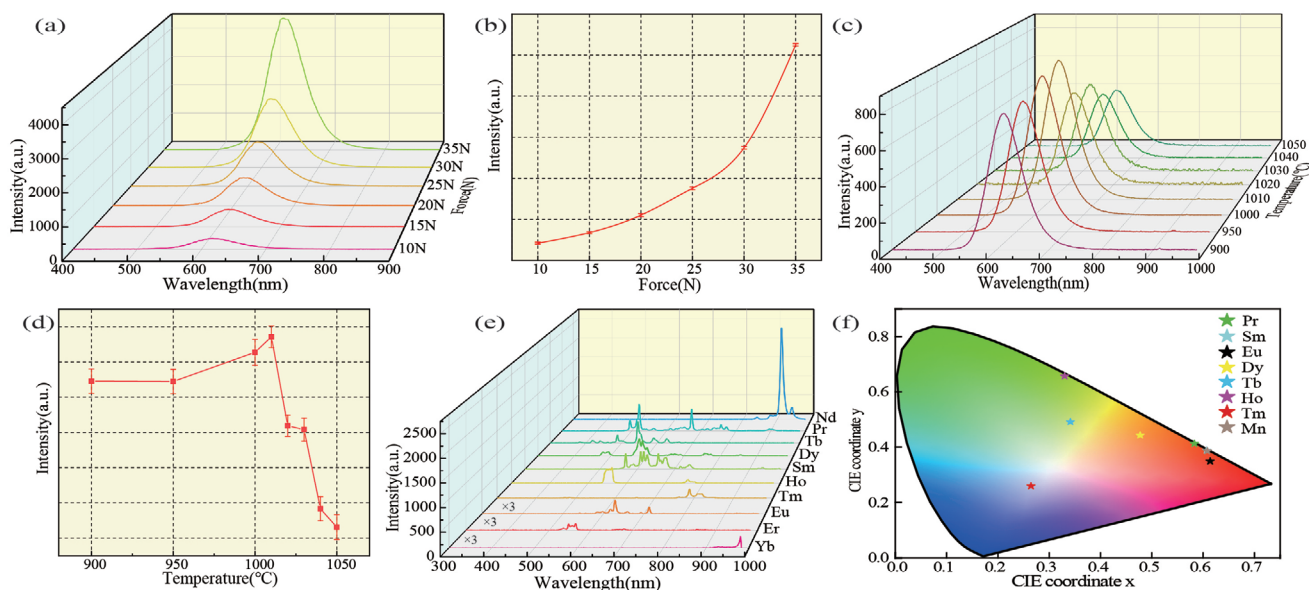

Figure 6. a) ML spectra of CaZnOS:Mn synthesized at 1000 °C under different forces; b) ML intensity integrals under different forces; c) ML spectra; d) intensity integrals under 20 N force; e) ML spectrum of Ln^{3+} doped CaZnOS under a force of 30 N; f) chromaticity coordinates of ML.

ADVANCED
SCIENCE NEWS
www.advancedsciencenews.com

NANO · MICRO
small
www.small-journal.com

Figure 6c shows the ML spectrum of samples synthesized at different temperatures under a force of 20 N, whereas Figure 6d shows the intensity integral diagram corresponding to Figure 6c.

When the temperature reaches 1010 °C, the ML intensity of the CaZnOS:Mn under the same force has the largest value. This may be attributed to the crystal anisotropy. CaZnOS has a hexagonal asymmetric crystal structure, and the c-axis is the crystal polarization axis. That is, if the crystal grows along the c-axis, it will be easier to trigger the internal potential to increase the light emission, as widely observed and reported for other semiconductors such as ZnO, GaN, and CdS.[51,52] This is consistent with the SEM morphology observed in the present study. The crystal shows a longer sheet structure and a trend of c-axis-preferred growth. This preferred trend facilitates the formation of the built-in potential under the action of an external force, which is conducive to the realization of ML emissions. In addition, it is related to the recent rate of ion diffusion and scattering in the high-temperature molten salts. Ion diffusion and scattering are competitive. When the temperature reaches a certain level, the optimal state is formed, and is conducive to a more uniform distribution of manganese ions in the crystal. This affects the uniformity of luminescence, and will eventually affect the overall intensity of the ML. The degree of external force in contact with the crystal is also related to the final luminous intensity of the crystals. This leads to the fact that the synthesis temperature of the sample with the best ML is not the highest temperature, but a moderate one. Figure 6e shows the ML spectra of the Ln^{3+}-doped CaZnOS. The ML configurations of the different doped samples are consistent with the samples synthesized by the traditional solid-phase method.[35] We extracted the chromaticity coordinates for the Ln^{3+}-doped and Mn^{2+}-doped CaZnOS samples from the ML spectra. As shown in Figure 6f, the different dopants can achieve different colors. This will provide a large number of alternative colors for the ML display, from visible to near-IR.

In addition, the ML spectra for the ZnS/CaZnOS:Mn heterojunction sample were recorded under different forces; the spectral range is basically the same as in our previous measured results; the ML spectra for the heterojunctions prepared by the MSS method are shown in Figure S13, Supporting Information. Because mechanoluminescent materials emit light under the action of force, they do not require light, such as UV or IR excitation accordingly, they have important application prospects for pressure imaging, electronic signatures, and information anti-counterfeiting. We can achieve an ML prototype device through screen printing. **Figure 7**a shows photographs of handwriting on the ML film, showing yellow, green, and red colors with the same host CaZnOS semiconductors doped with different luminescent lanthanide ions; all of the samples were prepared by our MSS method (see also Videos S1–S7, Supporting Information for details of the ML-lighting process). We also integrated the ML, PL, and long-lasting luminescence characteristics of the same material, and prepared a multi-modal lightweight print that does not easily crack and shows a multi-modal luminescence effect, as displayed in the multi-modality and new fluorescence. The crystals have important promising applications in the field of anti-counterfeiting (see Video S7, Supporting information). We show a novel screen-printed

butterfly pattern with delayed luminescence, different from ordinary fluorescence, in addition to having ML characteristics (Figure 7a–d); the patterns have a phosphorescent property (Figure 7e–j) with a delayed effect.

As a method of high energy excitation, X-rays are now widely used to excite fluorescent materials. Recent studies have shown that mechanoluminescent materials are usually accompanied by good X-ray excitation PL properties. Therefore, we further studied this feature systematically. When using X-rays to excite CaZnOS samples doped with different lanthanide ions, we can achieve intensive multi-color X-ray fluorescence, as shown in **Figure 8**. We chose the X-ray source operating at $U = 50$ kV and $I = 40$ µA as the excitation for obtaining the XEL spectra. It can be observed that the CaZnOS for different lanthanide ions will show different luminescence properties after being excited by X-rays. The inset picture in Figure 8 shows a fluorescence microscope photo-image of the X-ray excitation from the ML film. We set the exposure time to 2 s and the sensitivity (ISO) to 3200, and the image was captured in a darkroom environment. The different luminous intensities of the samples after excitation are directly reflected in the brightness and darkness of the physical image.

To further verify the feasibility of non-doped luminescence, we prepared un-doped CaZnOS samples and irradiated them with X-rays. A stronger yellow emission was observed, as shown in **Figure 9**. Figure 9a shows the X-ray excited PL spectrum and fluorescent microscope photo-image. We compared the intensity of commercial scintillation crystals under year-on-year conditions and irradiated the same dose of X-rays with the scintillator NaI:Tl, as commonly used in industry applications. Interestingly, the XEL integrated intensity of the undoped CaZnOS was higher than that of NaI:Tl. To compare the effects of the different doped lanthanide ions, we calculated the integrated intensity of the XEL spectrum, as shown in Figure 9b; as shown, the three doped samples, Pr^{3+}, Sm^{3+}, and Tb^{3+} (2 mol%) have relatively higher luminous intensities. This corresponds to the real picture. Next, we tested the XEL spectrum of CaZnOS doped with a low concentration (0.2 mol%). When the doping concentration decreases to an order of magnitude, the XEL spectra broadly show a spectrum ranging from 500 to 700 nm, whereas the intrinsic luminescence of the lanthanide ions is retained in other positions, and the doped ions can still be seen in the characteristic peak position, as shown in Figure 9e,f. Compared with the high concentration of lanthanide ions, the intrinsic emission peak of the lanthanide still shows a certain degree of suppression. Therefore, by adjusting the doping concentration, the luminescence of the host and lanthanide ions can be flexibly adjusted, thereby flexibly adjusting the color of the luminescence. This provides potential application value for future X-ray excited semiconductor display devices. To accurately obtain the chromaticity coordinates of the XEL for different lanthanide ions, we extracted the XEL spectra to calculate the chromaticity coordinates of each doping element, as shown in Figure 9d, allowing us to achieve multi-color X-ray fluorescence.

The current development of medical and industrial diagnostic technology has led to accelerated research on X-ray excitation scintillation systems.[53–58] For example, lanthanide ion-doped lead halide perovskite materials exhibit intensive X-ray excitation luminescence. However, they usually contain
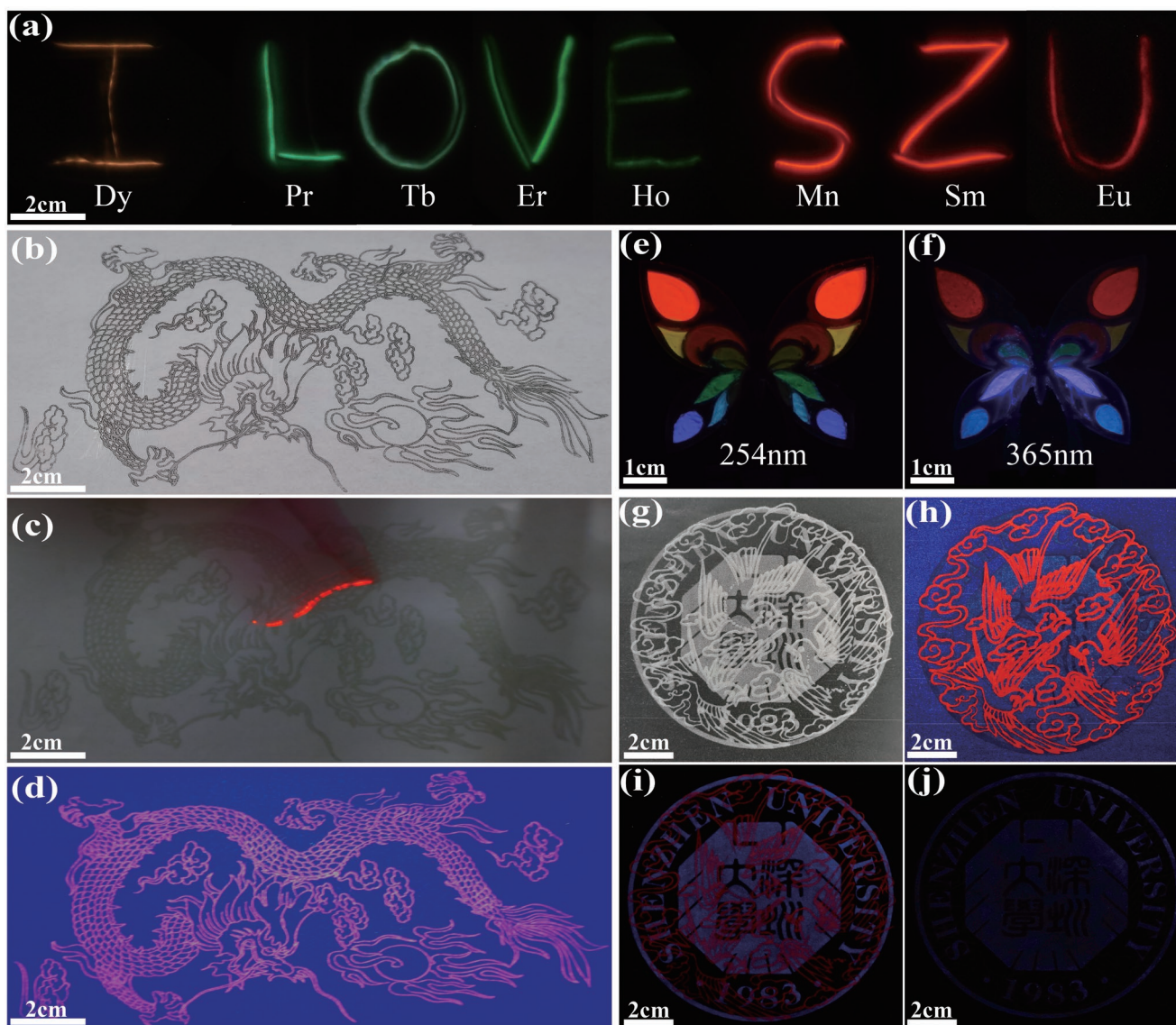
Figure 7. a) Photographs of handwriting on the ML film with a pen, showing yellow, green, and red color with CaZnOS:Sm, CaZnOS:Ho, and CaZnOS:Mn powders prepared by the MSS method, we set the exposure time of the camera to 3 s and the sensitivity to 1000; b–d) we use CaZnOS:Mn to screen print a pattern drawn on ordinary A4 paper and shoot it under an incandescent lamp; we use a pen to slide on the pattern. A very bright luminescence can be seen, based on irradiating a pattern with a 254 nm UV lamp; e,f) irradiating a butterfly mold with a 254 and 365 nm UV lamp, respectively, where the butterfly mold is filled with different samples; g–j) overlapping the logo of Shenzhen University painted by CaZnOS:Bi with the bird painted by CaZnOS:Mn by using screen printing technology, shoot the pattern irradiated with a 254 nm UV lamp under an incandescent lamp; i) the pattern when the UV lamp is turned off; j) the picture after 5 s after turning off the UV lamp.

a high amount of lead, silver, or even a high concentration of heavy lanthanide ions to form the matrix, with long-term adverse effects on the environment, as well as high costs for the raw material and synthesis; they also suffer from poor stability and are not easy to store in high-temperature and humid environments, which is not conducive to wide application in the market. We believe that our material is a biocompatible and multifunctional fluorescent material. With the introduction of the nano-synthesis process into the system, uniform monodisperse colloids could be obtained, such as 0D quantum dots, or 2D single-layer semiconductors could be realized by the addition of a liquid-phase stripping process.

3. Conclusions

In this work, a series of high quality monodisperse CaZnOS single crystals were synthesized by a simple MSS method in air for the first time. We can not only fine-tune the morphology of the crystal by simply controlling the annealing temperature, but can also successfully achieve multi-luminescence of a large number of transition metal or lanthanide ions. By using different dopants, we can achieve versatility in the luminescence for doped CaZnOS-based semiconductors in terms of ML, PL, and XEL, and for the first time, we discovered that un-doped CaZnOS has a higher XEL luminous intensity
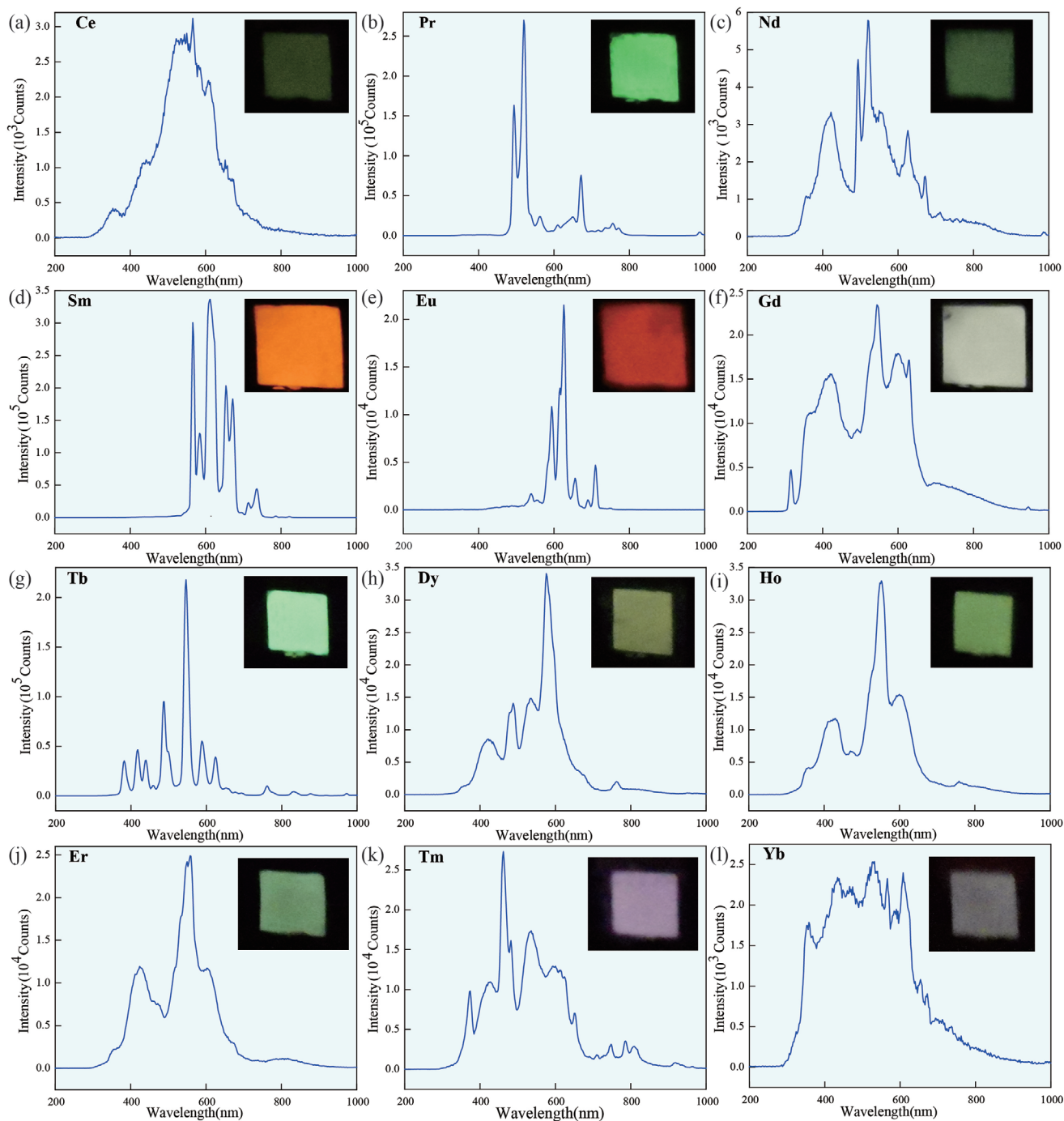
ADVANCED
SCIENCE NEWS
www.advancedsciencenews.com

NANO · MICRO
small
www.small-journal.com

Figure 8. X-ray excitation luminescence (XEL) spectra of CaZnOS doped with different lanthanides. The inset is the corresponding photographs taken with a digital camera. The size of the light-emitting area is a rectangle of 3 cm × 3 cm; a) Ce; b) Pr; c) Nd; d) Sm; e) Eu; f) Gd; g) Tb; h) Dy; i) Ho; j) Er; k)Tm; and l) Yb, respectively, the doping concentration of all of the lanthanide ions is 2 mol%, indicating these crystals can achieve multi-color luminescence under low-dose X-ray irradiation.

relative to standard commercial NaI:Tl; moreover, other elements are mixed to have a certain inhibitory effect on XEL, facilitating the moderation of the spectra of different colors as a X-ray detection and imaging material. As a new type of multifunctional piezo-photonic third-generation semiconductor with environmentally friendly and biocompatible elements such as Ca, Zn, O, and S, the multi-luminescent properties of

CaZnOS semiconductors prepared by our method have great potential for multifunctional advanced lighting and imaging, sensing, and energy applications. This method opens a door for the rapid and high-yield synthesis of oxidation prone materials such as 2D layered structure, such as disulfide or black phosphorus, chalcogenide, or oxysulfide semiconductor crystals with functionalities.[40–42]
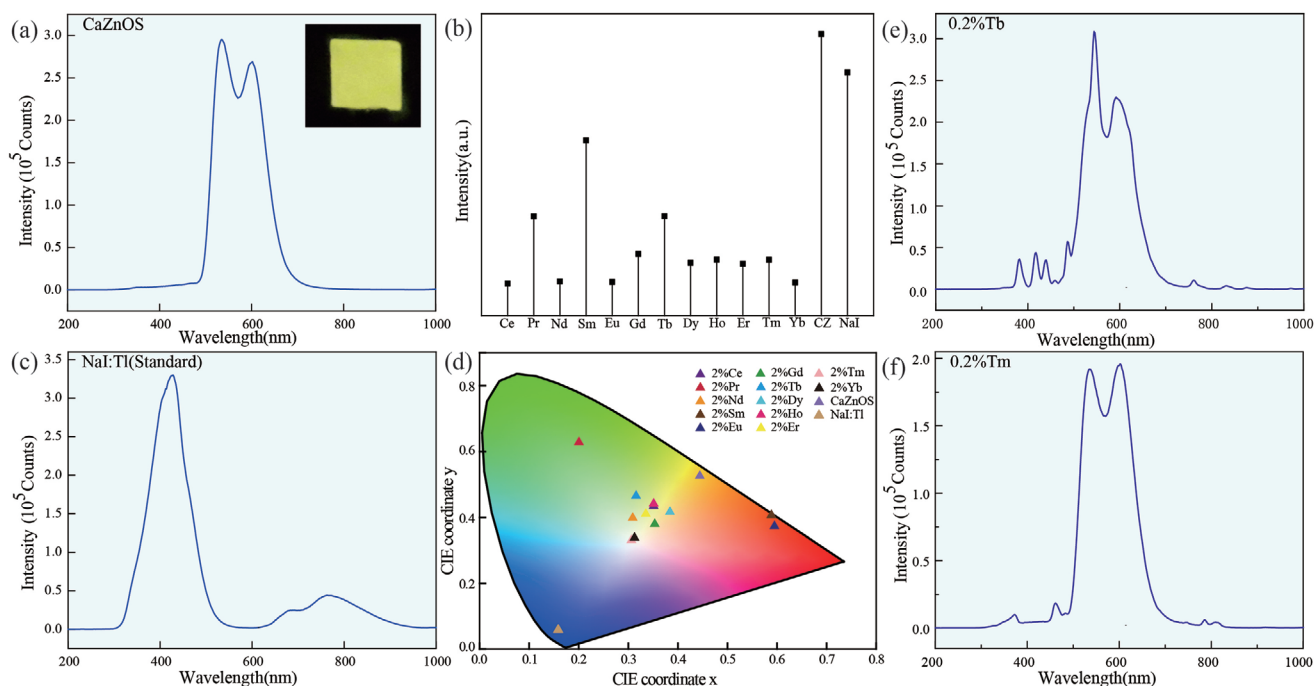
Figure 9. a) CaZnOS; b) the integrated intensity calculated from the XEL spectrum, CZ represents undoped CaZnOS; c) NaI:Tl emission spectrum; d) under the excitation of an X-ray source with $U = 50$ kV and $I = 40$ μA, chromaticity coordinates calculated by XEL spectrum; e) XEL spectrum of CaZnOS:Tb (0.2%); f) XEL spectrum of CaZnOS:Tm (0.2%).

4. Experimental Section

Molten Salt Shielded Method Preparation of CaZnOS:Mn²⁺/Ln³⁺: Monodisperse CaZnOS sheet-like powders were prepared by the MSS method, as described below. The raw chemicals included CaCO₃ (purity > 99%, Sigma), ZnS (purity 99.99%, Aladdin), and MnCl₂·4H₂O, LnCl₃·H₂O, and NaCl (purity 99.8%, Aladdin). First, the CaCO₃ was placed in a crucible for alumina; then, it was placed in a high-temperature muffle furnace heated by a resistance wire kept at 1000 °C for 4 h to decompose and obtain pure CaO. Then, 5 g of ZnS and MnCl₂·4H₂O/LnCl₃ (≈2 mol% to ZnS)/BiCl₃/CuO/PbO were evenly mixed with ethanol as the dispersion medium, providing detailed melt-salt compositions. After volatilizing and drying, the prepared CaO was added (with the same molar ratio as ZnS) into the mixture, ground for 10 min. The mixture was placed into a corundum crucible, and covered with 15 g NaCl on the upper surface of the mixture; it was then carefully compacted, and placed in a crucible in the air atmosphere of the high-temperature furnace and sintered at 900–1100 °C for 4 h. After the sintered product was naturally cooled to room temperature in the furnace, the NaCl solid crystals embedded in the sample were washed with deionized water, and finally dried in a drying oven at 80 °C to obtain the powder for subsequent characterization and usage. The flow diagram is shown in Figure 1. The detailed design of the experiment is presented in Table S1, Supporting information.

Production of Mechanoluminescent Film: As a typical experimental process, 0.3 g of the sample and 0.06 g of a UV curing adhesive (LEAFTOP 9307) were weighed, placed it into 10 mL centrifuge tube. Then, 9 mL of absolute ethanol was added and the mixture was shaken fully to make the sample mix evenly with UV curing adhesive, before quickly being transferred into a 3 cm × 3 cm rectangular mold. An abrasive tool was placed in the inner layer laminating film (Deli, No. 3817). One layer of each protective film was ≈15 microns thick and covered with thermoplastic on one side, and the mold was placed in a drying oven at 80 °C. After all of the ethanol was dried, the mold was removed, the protective film was sealed, and the sample was irradiated with an UV lamp to cure the adhesive. The ML film was

used for subsequent ML tests and X-ray irradiation to obtain XEL spectra.

Screen Printing Details: The masked plate patterns (17 cm × 8 cm, 150 mesh), including the logo of Shenzhen University, dragon, magpie, and Wechat QR code, were customized for screen printing. The plain UV ink and phosphor were mixed in the ratio of 10:1 and blade-coated evenly to the screen, which attached the designed patterns on the top side, while an A4 paper closed up the bottom side. After blade-coating and painting over and over again, the ML ink pattern wrapped with phosphor will appear on the paper to form the printed pattern. The thickness of the pattern was controlled by the number of times of coating. Finally the paper was put in an oven drying at 80 °C for 5 min.

Materials Characterization: XRD was performed using a high-resolution X-ray diffractometer. SEM and EDS were performed using a Thermo APREO S instrument to observe the morphology and elemental distributions of the samples. High-resolution TEM Images were characterized by STEM HADDF-STEM (Titan3 Cubed Themis G2). The PL spectra and QY were measured using an Edinburgh FSL1000 spectrometer equipped with an integrating sphere. An X-ray source working under $U = 50$ kV and $I = 40$ μA was used as the excitation source to obtain the XEL spectrum. The ML spectrum was recorded using a self-made measuring instrument equipped with a linear motor, digital push-pull instrument, and QE65pro optical fiber spectrometer (Ocean Optics). The ML film was pasted on a quartz glass sheet. On the front of the quartz glass sheet, a digital push-pull instrument with metal accessories was fixed on a platform; the platform was connected to a linear motor, and on the back, the optical fiber was connected to the fiber spectrometer. The pressure of the metal accessories on the ML film was adjusted by the push-pull meter, and the motion of the platform was controlled by a linear motor. In the test process, the movement of the stainless steel sliding head metal bearing on the multilayer film produced light emissions, and the optical fiber synchronously collected signals. By applying different forces and selecting different points, each force was measured more than five times to ensure the accuracy of the data when obtaining the ML spectra.

Supporting Information

Supporting Information is available from the Wiley Online Library or from the author.

Acknowledgements

Conflict of Interest

The authors declare no conflict of interest.

Data Availability Statement

The data that support the findings of this study are available from the corresponding author upon reasonable request.

Keywords

[1] S. M. Jeong, S. Song, S. K. Lee, B. Choi, *Appl. Phys. Lett.* **2013**, *102*, 361.
[2] X. D. Wang, H. L. Zhang, R. M. Yu, L. Dong, D. F. Peng, A. H. Zhang, Y. Zhang, H. Liu, C. F. Pan, Z. L. Wang, *Adv. Mater.* **2015**, *27*, 2324.
[3] X. D. Wang, D. F. Peng, B. L. Huang, C. F. Pan, Z. L. Wang, *Nano Energy* **2019**, *55*, 389.
[4] Y. X. Zhuang, R. J. Xie, *Adv. Mater.* **2021**, *33*, 2005925.
[5] B. Chen, X. Zhang, F. Wang, *Acc. Mater. Res.* **2021**, *2*, 364.
[6] X. X. Yang, R. Liu, X. H. Xu, Z. C. Liu, M. Z. Sun, D. F. Peng, C. N. Xu, B. L. Huang, D. Tu, *Small* **2021**, *17*, 2103441.
[7] C. X. Hu, L. Cheng, Z. Wang, Y. B. Zheng, S. Bai, Y. Qin, *Small* **2016**, *12*, 1315.
[8] X. L. Chen, X. M. Li, J. Y. Shao, N. L. An, H. M. Tian, C. Wang, T. Y. Han, L. Wang, B. H. Lu, *Small* **2017**, *13*, 1604245.
[9] C. H. Liow, X. Lu, C. F. Tan, K. H. Chan, K. Y. Zeng, S. Z. Li, G. W. Ho, *Small* **2018**, *14*, 1702268.
[10] K.-H. Kim, K. Y. Lee, J.-S. Seo, B. Kumar, S.-W. Kim, *Small* **2011**, *7*, 2577.
[11] D. F. Peng, C. F. Wang, R. H. Ma, S. H. Mao, S. C. Qu, Z. B. Ren, S. Golovynskyi, C. F. Pan, *Sci. Bull.* **2021**, *66*, 206.
[12] C. F. Wang, D. F. Peng, C. F. Pan, *Sci. Bull.* **2020**, *65*, 1147.
[13] G. S. Hong, *Science* **2020**, *369*, 638.
[14] X. Wu, X. J. Zhu, P. Chong, J. L. Liu, L. N. Andre, K. S. Ong, K. B. jr., A. I. Mahdi, J. C. Li, L. E. Fenno, H. L. Wang, G. S. Hong, *Proc. Natl. Acad. Sci. USA* **2019**, *116*, 26332.
[15] S. Aman, J. Tomas, *Powder Technol.* **2004**, *146*, 147.
[16] P. Jha, A. Khare, P. Singh, S. K. Nema, *J. Lumin.* **2020**, *222*, 117176.
[17] Y. J. Xie, Z. Li, *Chem* **2018**, *4*, 943.
[18] J. C. Zhang, X. S. Wang, G. Marriott, C. N. Xu, *Prog. Mater. Sci.* **2019**, *103*, 678.
[19] R. H. Ma, X. Y. Wei, C. F. Wang, S. H. Mao, B. Chen, Y. H. Shao, Y. Fu, K. Y. Yan, D. F. Peng, *J. Lumin.* **2021**, *232*, 117838.
[20] C. N. Xu, T. Watanabe, M. Akiyama, X. G. Zheng, *Appl. Phys. Lett.* **1999**, *74*, 1236.
[21] Y. Oshima, A. Nakamura, K. Matsunaga, *Science* **2018**, *360*, 772.
[22] J. H. Hao, C. N. Xu, *MRS Bull.* **2018**, *43*, 965.
[23] C. C. Trowbridge, *Science* **1904**, *19*, 825.
[24] G. Alzetta, N. Minnaja, S. Santucci, R. N. Cimento, **1962**, *23*, 910.
[25] D. F. Peng, Y. Jiang, H. B. L., D. Y. Y., J. X. Zhao, X. Zhang, R. H. Ma, S. Golovynskyi, B. Chen, F. Wang, *Adv. Mater.* **2020**, *32*, 16.
[26] S. M. Jeong, S. Song, H. Kim, *Nano Energy* **2016**, *21*, 154.
[27] L. Zhang, K. Y. Shi, Y. L. Wang, L. Su, G. Q. Yang, B. L. Huang, J. Kong, X. Dong, Z. L. Zhong, *Nano Energy* **2021**, *85*, 106005.
[28] X. D. Wang, R. Ling, Y. F. Zhang, M. L. Que, Y. Y. Peng, C. F. Pan, *Nano Res.* **2018**, *11*, 1967.
[29] F. L. Wang, F. L. Wang, X. D. Wang, S. C. Wang, J. F. Jiang, Q. L. Liu, X. T. Hao, L. Han, J. J. Wang, C. F. Pan, H. Liu, Y. H. Sang, *Nano Energy* **2019**, *63*, 103861.
[30] V. K. Chandra, B. P. Chandra, P. Jha, *Appl. Phys. Lett.* **2013**, *103*, 161113.
[31] M. V. Mukhina, J. Tresback, J. C. Ondry, A. Akey, A. P. Alivisatos, N. Kleckner, *ACS Nano* **2021**, *15*, 4115.
[32] J. C. Zhang, C. N. Xu, S. Kamimura, Y. Terasawa, H. Yamada, X. Wang, *Opt. Express* **2013**, *21*, 12976.
[33] T. W. Kuo, W. R. Liu, T. M. Chen, *Opt. Express* **2010**, *18*, 8187.
[34] D. Tu, C. N. Xu, A. Yufio, A. Yoshida, *Light: Sci. Appl.* **2015**, *4*, e356.
[35] Y. Y. Du, Y. Jiang, T. Y. Sun, J. X. Zhao, B. L. Huang, D. F. Peng, F. Wang, *Adv. Mater.* **2019**, *31*, 1807062.
[36] W. Wang, D. F. Peng, H. L. Zhang, X. H. Yang, C. F. Pan, *Opt. Commun.* **2017**, *395*, 24.
[37] L. J. Li, L. Wondraczek, L. H. Li, Y. Zhang, Y. Zhu, M. Y. Peng, C. B. Mao, *ACS Appl. Mater. Interfaces* **2018**, *10*, 14509.
[38] M. Li, J. Lu, K. Luo, Y. B. Li, K. K. Chang, K. Chen, J. Zhou, J. Rosen, L. Hultman, P. Eklund, P. O. Å. Persson, S. Y. Du, Z. F. Chai, Z. R. Huang, Q. Huang, *J. Am. Chem. Soc.* **2019**, *141*, 4730.
[39] V. Srivastava, V. Kamysbayev, L. Hong, E. Dunietz, R. F. Klie, D. V. Talapin, *J. Am. Chem. Soc.* **2018**, *140*, 12144.
[40] A. Dash, R. Vaßen, O. Guillon, J. Gonzalez-Julian, *Nat. Mater.* **2019**, *18*, 465.
[41] Y. B. Li, H. Shao, Z. F. Lin, J. Lu, L. Y. Liu, B. Duployer, P. O. Å. Persson, P. Eklund, L. Hultman, M. Li, K. Chen, X. H. Zha, S. Y. Du, P. Rozier, Z. F. Chai, E. Raymundo-Piñero, P. L. Taberna, P. Simon, Q. Huang, *Nat. Mater.* **2020**, *19*, 894.
[42] V. Kamysbayev, A. S. Filatov, H. C. Hu, X. Rui, F. Lagunas, D. Wang, R. F. Klie, D. V. Talapin, *Science* **2020**, *369*, 979.
[43] C. Wang, Y. Yu, Y. H. Yuan, C. Y. Ren, Q. Y. Liao, J. Q. Wang, Z. F. Chai, Q. Q. Li, Z. Li, *Matter* **2020**, *2*, 181.
[44] R. R. Petit, S. E. Michels, A. Feng, P. F. Smet, *Light: Sci. Appl.* **2019**, *8*, 124.
[45] J. C. Zhang, L. Z. Zhao, Y. Z. Long, H. D. Zhang, B. Sun, W. P. Han, X. Yan, X. S. Wang, *Chem. Mater.* **2015**, *27*, 7481.
[46] T. Sambrook, C. F. Smura, S. J. Clarke, *Inorg. Chem.* **2007**, *46*, 2571.
[47] S. A. Petrova, V. P. Mar'evich, R. G. Zakharov, E. N. Selivanov, V. M. Chumarev, L. Y. Udoeva, *Dokl. Chem.* **2003**, *393*, 255.
[48] B. L. Huang, *Phys. Chem. Chem. Phys.* **2016**, *18*, 25946.

[49] B. L. Huang, D. F. Peng, C. F. Pan, *Phys. Chem. Chem. Phys.* **2017**, *19*, 1190.

[50] D. Tu, C. N. Xu, S. Kamimura, Y. Horibe, H. Oshiro, L. Zhang, Y. Ishii, K. Hyodo, G. Marriott, N. Ueno, X. G. Zheng, *Adv. Mater.* **2020**, *32*, 1908083.

[51] C. F. Pan, L. Dong, G. Zhu, S. M. Niu, R. M. Yu, Q. Yang, Y. Liu, Z. L. Wang, *Nat. Photonics* **2013**, *7*, 752.

[52] C. F. Pan, J. Y. Zhai, Z. L. Wang, *Chem. Rev.* **2019**, *119*, 9303.

[53] L. Lu, M. Z. Sun, Q. Y. Lu, T. Wu, B. L. Huang, *Nano Energy* **2021**, *79*, 105437.

[54] P. Pei, Y. Chen, C. X. Sun, Y. Fan, Y. M. Yang, X. Liu, L. F. Lu, M. Y. Zhao, H. X. Zhang, D. Y. Zhao, X. G. Liu, F. Zhang, *Nat. Nanotechnol.* **2021**, *16*, 1011.

[55] Z. J. Zhang, A. Feng, X. Y. Sun, K. Guo, Z. Y. Man, J. T. Zhao, *J. Alloys Compd.* **2014**, *592*, 73.

[56] Z. C. Zeng, B. L. Huang, X. Wang, L. Lu, Q. Y. Lu, M. Z. Sun, T. Wu, T. F. Ma, J. Xu, Y. S. Xu, S. A. Wang, Y. P. Du, C. H. Yan, *Adv. Mater.* **2020**, *32*, 2004506.

[57] X. Y. Ou, X. Qin, B. L. Huang, J. Zan, Q. X. Wu, Z. Z. Hong, L. L. Xie, H. Y. Bian, Z. G. Yi, X. F. Chen, Y. M. Wu, X. R. Song, J. Li, Q. S. Chen, H. H. Yang, X. G. Liu, *Nature* **2021**, *590*, 410.

[58] Q. S. Chen, J. Wu, X. Y. Ou, B. L. Huang, J. Almutlaq, A. A. Zhumekenov, X. W. Guan, S. Y. Han, L. L. Liang, Z. G. Yi, J. Li, X. J. Xie, Y. Wang, Y. Li, D. Y. Fan, D. B. L. Teh, A. H. All, O. F. Mohammed, O. M. Bakr, T. Wu, M. Bettinelli, H. H. Yang, W. Huang, X. G. Liu, *Nature* **2018**, *561*, 88.